Chemical Science

ROYAL SOCIETY OF CHEMISTRY

EDGE ARTICLE

View Article Online
View Journal | View Issue

Cite this: *Chem. Sci.*, 2021, **12**, 10290

All publication charges for this article have been paid for by the Royal Society of Chemistry

Hydroxyl improving the activity, selectivity and stability of supported Ni single atoms for selective semi-hydrogenation†

Minzhen Jian,[a] Jin-Xun Liu *[a] and Wei-Xue Li *[ab]

Atomically dispersed metal catalysts with high atomic utilization and selectivity have been widely studied for acetylene semi-hydrogenation in excess ethylene among others. Further improvements of activity and selectivity, in addition to stability and loading, remain elusive due to competitive adsorption and desorption between reactants and products, hydrogen activation, partial hydrogenation *etc.* on limited site available. Herein, comprehensive density functional theory calculations have been used to explore the new strategy by introducing an appropriate ligand to stabilize the active single atom, improving the activity and selectivity on oxide supports. We find that the hydroxyl group can stabilize Ni single atoms significantly by forming $Ni_1(OH)_2$ complexes on anatase TiO_2(101), whose unique electronic and geometric properties enable high performance in acetylene semi-hydrogenation. Specifically, $Ni_1(OH)_2$/TiO_2(101) shows favorable acetylene adsorption and promotes the heterolytic dissociation of H_2 achieving high catalytic activity, and it simultaneously weakens the ethylene bonding to facilitate subsequent desorption showing high ethylene selectivity. Hydroxyl stabilization of single metal atoms on oxide supports and promotion of the catalytic activity are sensitive to transition metal and the oxide supports. Compared to Co, Rh, Ir, Pd, Pt, Cu, Ag and Au, and anatase ZrO_2, IrO_2 and NbO_2 surfaces, the optimum interactions between Ni, O and Ti and resulted high activity, selectivity and stability make $Ni_1(OH)_2/TiO_2$(101) a promising catalyst in acetylene hydrogenation. Our work provides valuable guidelines for utilization of ligands in the rational design of stable and efficient atomically dispersed catalysts.

Received 8th June 2021
Accepted 19th June 2021

DOI: 10.1039/d1sc03087f

rsc.li/chemical-science

Introduction

Raw ethylene generated by catalytic cracking generally contains 1% acetylene, which has to be removed or reduced to a few ppm to avoid downstream catalyst poisoning and the degradation of polyethylene quality during ethylene polymerization.[1–5] The selective hydrogenation of trace acetylene toward ethylene is the most widely used route in the removal of acetylene from the ethylene feed. The major side reaction in acetylene hydrogenation is the generation of undesirable ethane by ethylene hydrogenation and the coupling of C_2 species to a green oil blocking the active site. Correspondingly, an efficient catalyst for selective acetylene hydrogenation requires suppressing complete hydrogenation and inhibiting C–C coupling and carbon deposition.

Pd is considered as a state-of-the-art catalyst for selective hydrogenation of acetylene, but its high cost and poor selectivity toward ethylene inevitably limits its widespread application.[6,7] Belonging to the same group as Pd in the periodic table, Ni metal also shows excellent hydrogenation activity.[8,9] The earth abundant and low cost Ni can be considered as an alternative to Pd-based catalysts. However, Ni metal can oligomerize hydrocarbon reactants, which subsequently reduces catalytic selectivity in acetylene hydrogenation towards ethylene.[10–12] Improved selectivity for acetylene hydrogenation towards ethylene can be achieved by alloying Ni with inactive metals, such as Zn,[13–17] Cu,[18–20] Au,[21–23] Ga[24–26] and Sn,[27,28] to form bimetallic particles. Nevertheless, the resulting bimetallic catalysts with the presence of an extended ensemble are not free from the formation of ethane and oligomers. Previous studies revealed that three neighboring Ni atoms can trigger oligomerization,[8,29] and isolation of the Ni atoms would suppress oligomerization and improve coke resistance.[30] Therefore, oligomer and coke formation is expected to decrease dramatically on atomically dispersed Ni-based catalysts, which might be promising for acetylene semi-hydrogenation.

Atomically dispersed catalysts received wide attention due to their complete exposure of the active metal and demonstrated

[a]*Department of Chemical Physics, School of Chemistry and Materials Science, University of Science and Technology of China, Hefei, Anhui 230026, China. E-mail: wxli70@ustc.edu.cn; jxliu86@ustc.edu.cn*

[b]*Hefei National Laboratory for Physical Sciences at the Microscale, Hefei, Anhui 230026, China*

† Electronic supplementary information (ESI) available. See DOI: 10.1039/d1sc03087f

high activity and selectivity in various reactions.[40,41] Compared to traditional nanocatalysts on supports, the confined environment of atomically dispersed catalysts with distinct electronic and geometric structures influences reactant adsorption, activation, reaction on the surface as well as the desorption of desired products dramatically, for achieving the corresponding catalytic activity and selectivity. Compared to stronger adsorption of acetylene than ethylene on palladium particles, acetylene adsorption on atomically dispersed catalysts is weak,[31] which would lower the overall activity of acetylene semi-hydrogenation, considering rather low acetylene partial pressure under practical reaction conditions. Improving acetylene bonding but not ethylene bonding, which would prevent ethylene desorption and decrease corresponding selectivity otherwise, is a prerequisite. There have been considerable efforts devoted to modifying the chemical environment of single metal atoms with altered electronic and geometric structures to achieve better activity and selectivity.[32–37] To the best of our knowledge, there are still only a few experimental studies reported on acetylene semi-hydrogenation over the atomically dispersed Ni catalyst,[38,39] let alone on the chemical modification of atomically dispersed Ni catalysts but addressed in present work theoretically.

Atomically dispersed metal catalysts might often suffer from poor H_2 activation due to their relatively weak bonding compared to alternative reactants and/or intermediates involved in hydrogenation reactions. Efficient activation of H_2 without triggering the undesirable side reaction is another prerequisite.[42] Zheng and co-workers[43] found that on an ethylene glycolate (EG)-stabilized Pd single atom on ultrathin TiO_2 nanosheets, heterolytic H_2 dissociation occurs at the Pd–O interface with extremely high activity. The Karim group[44] found that a CO–Ir complex anchored on a $MgAl_2O_4$ support is the active site for CO oxidation at low temperature. New interfacial sites formed for the metal–ligand complexes on supports, found for hydroxyl (OH) as well,[45–47] could be explored. Moreover, the presence of ligands can improve the stability of atomically dispersed metal catalysts by forming energetically more favorable complexes;[47–50] It is one of the critical aspects for practical application. Though OH is widely present in catalytic systems, the question of whether and how OH could improve H_2 activation and acetylene semi-hydrogenation, in addition to stability, over a Ni single atom catalyst remains open.

Supports play a vital role in enhancing the stability and catalytic performance of a single atom catalyst. The anatase titanium oxide (TiO_2) phase, which is often used in acetylene semi-hydrogenation,[51,52] is well known for its high-reactivity in photocatalysis and stability in nanocrystals due to the exposure of more (101) facet with a low surface free energy.[53–56] In the present work, we studied OH modulated Ni single atom catalysts on anatase TiO_2(101) for acetylene semi-hydrogenation by density functional theory (DFT) calculations. We first studied how Ni_1 atoms were stabilized in different Ni_1-hydroxyl complexes on TiO_2 under steaming conditions. Energetically favorable $Ni_1(OH)_2/TiO_2$ with right energetics for acetylene adsorption and ethylene desorption was identified. Facile H_2 activation and selective hydrogenation promoted by the OH ligand were revealed. We clarify the origin of the high performance of $Ni_1(OH)_2/TiO_2$ in acetylene semihydrogenation by comparing with other transition metal atoms (Co, Rh, Ir, Pd, Pt, Cu, Ag and Au) and oxide supports (ZrO_2, NrO_2 and IrO_2). The present work provides valuable insights into the critical role of ligands in stabilizing atomically dispersed metal atoms on supports and enhancing the catalytic activity and selectivity.

Computational methods

Spin-polarized periodic DFT calculations were performed by using the Vienna *Ab initio* Simulation Package (VASP).[57,58] The exchange-correlation interaction is described by the optB86b-vdW functional.[59] The GGA+*U* approach was used to treat the strong on-site Coulomb interaction of localized electrons in TiO_2, NbO_2, ZrO_2 and IrO_2 with corresponding *U* values of 3, 2, 4, 1 eV for Ti, Nb, Zr and Ir, respectively, according to previous literature.[60–62] The core electrons were represented by the projector augmented wave (PAW) method[63] and the Kohn–Sham valence states [Ti($3d^2$, $4s^2$), Zr($4d^2$, $5s^2$), Nb($4p^6$, $4d^4$, $5s^1$), Ir($4f^{14}$, $5d^7$, $6s^2$), Ni($4s^2$, $3d^8$), O($2s^2$, $2p^4$), C($2s^2$, $2p^2$), and H($1s^1$)] were expanded in a plane-wave basis set with a kinetic energy cutoff of 400 eV. The convergence threshold for electronic self-consistent interactions is 10^{-5} eV. Spin-polarized calculations were incorporated in the geometry optimization and transition state search. Structure optimization and transition state search were converged to the extent that the maximum residual force was 0.02 eV $Å^{-1}$ and 0.05 eV $Å^{-1}$ in all relaxed degrees of freedom, respectively. Transition states were determined by the climbing image nudged elastic band (CI-NEB) method[64,65] and improved dimer method,[66] then verified to possess only one vibrational mode with a negative curvature in the direction of the bond breaking or forming process. The vibrational frequencies and corresponding normal modes were calculated based on the numerical calculations of the second derivatives of the potential energy surface based on the harmonic oscillator approximation. For the vibrational frequencies and modes calculations, all the $Ni_1(OH)_2$ active center and adsorbates were allowed to relax. The adsorbates and the Ni coordinated with adsorbates were allowed to relax during the frequency calculations on the Ni (111) surface.

A $p(2 \times 3)$ slab including six O–Ti–O atomic layers was used to model the anatase TiO_2(101) surface, where the top three O–Ti–O atomic layers in the supercell including the Ni atom were fully relaxed. The crystal phases with the same space group as anatase TiO_2 were chosen for the other metal oxides (ZrO_2, NbO_2, and IrO_2) employing the same supercell and layer as TiO_2(101). The vacuum space perpendicular to the surface was 20 Å, which was enough to avoid interactions between the neighboring slabs. The artificial mirror interaction along the *z*-direction was avoided by dipole correction. The surface Brillouin zone was sampled on a $(3 \times 3 \times 1)$ Monkhorst–Pack *k*-point grid. The adsorption energy without Gibbs free energy correction was calculated by $\Delta E_{ads} = E_{tot} - E_{slab} - E_{gas}$, where E_{tot} and E_{slab} refer to the energy of the slab with adsorbates and the energy of the clean slab, respectively, and E_{gas} refers to the energy of the involved gas phase adsorbates in a neutral state.

The reaction energy and activation energy barrier without Gibbs free energy correction were calculated as $\Delta E_{rxn} = E_{FS} - E_{IS}$ and $E_a = E_{TS} - E_{IS}$, where E_{IS}, E_{FS} and E_{TS} refer to the energy of the initial state (IS), final state (FS) and corresponding transition state (TS), respectively.

The Gibbs free energies of all the species were corrected by:

$$G(T) = E_{DFT} + ZPE + H(T) - TS(T) \quad (1)$$

where E_{DFT} is the total electronic energy of the species obtained by DFT calculations at 0 K; ZPE is the zero-point energy. $H(T)$ and $S(T)$ are the enthalpy and entropy of the species at temperature T.

The entropy and enthalpy of the adsorbed species at temperature T were estimated according to the harmonic oscillator approximation following the equation:

$$S(T) = k_B \sum_i^{3N} \left[\frac{h\nu_i}{k_B T(e^{h\nu_i/k_B T} - 1)} - \ln(1 - e^{-h\nu_i/k_B T}) \right] \quad (2)$$

where k_B is Boltzmann's constant, h is the Planck constant, and N is the number of atoms in the adsorbates or gas.

$$H(T) = U(T) + \gamma RT = k_B T \sum_i^{3N} \frac{h\nu_i}{k_B(e^{h\nu_i/k_B T} - 1)} + \gamma RT \quad (3)$$

where U is the internal energy at temperature T. R is the molar gas constant. γ equals 0 for surface adsorbates, and 1 for the gaseous molecule.

Thus, the Gibbs free energy change for the surface elementary reaction and adsorption was calculated as:

$$\Delta G = \Delta E + \Delta ZPE + \Delta H - T\Delta S \quad (4)$$

where ΔE denotes the total electronic energy change based on DFT calculations.

Results and discussion

Structure and stability of Ni_1/TiO_2 and $Ni_1(OH)_2/TiO_2$ catalysts

An efficient catalyst for selective semi-hydrogenation should consist of spatially isolated sites to avoid C–C coupling or C–C cleavage in the formation of green oil or coke. In the present work, the atomically dispersed non-noble Ni metal on the anatase-TiO_2(101) surface, namely Ni_1/TiO_2, was studied. The most stable structure for Ni single atom adsorption on TiO_2 is given in Fig. S1.† The Ni single atom prefers to anchor on the hollow site by binding three O atoms in TiO_2(101) with the binding energy of −3.62 eV, which is in line with a previous report[67] and similar to the value of single Pt or Pd atom adsorption on the anatase TiO_2(101) surface.[68,69] Hydroxyl (OH) is a common species on the oxide surface, especially in the presence of H_2 and/or steaming conditions. Therefore, OH can be used as a suitable candidate ligand to modulate the stability and electronic structure of Ni atoms. When treating Ni_1/TiO_2 with steam, one H_2O molecule can be decomposed at the Ni site forming two OH groups binding with the Ni atom, namely $Ni_1(OH)_2/TiO_2$ (Fig. S1†). H_2O dissociation at the Ni_1/TiO_2 catalyst to generate two OH ligands is exothermic by −0.35 eV with the activation barrier of 0.96 eV (Fig. 1A). Therefore, the formation of the stable $Ni_1(OH)_2/TiO_2$ form is thermodynamically and kinetically feasible under the reaction conditions at T = 360 K and $P(H_2O)$ = 1 atm. The two OH ligands combined with the Ni atom are in a linear configuration in the $Ni_1(OH)_2/TiO_2$ catalyst leaving side space for acetylene hydrogenation. The stabilities of Ni_1/TiO_2, $Ni_1(OH)\_H/TiO_2$ and $Ni_1(OH)_2/TiO_2$ as a function of temperature and pressure of H_2O are shown in Fig. 1B. Ni_1/TiO_2 is only present at a high temperature or low pressure of H_2O. However, $Ni_1(OH)\_H/TiO_2$ and $Ni_1(OH)_2/TiO_2$ can be formed at a low temperature and high pressure of H_2O. Regardless of the temperature and pressure of water, the Gibbs free energy difference between the formation of $Ni_1(OH)\_H/TiO_2$ and $Ni_1(OH)_2/TiO_2$ is 0.01 eV, indicating $Ni_1(OH)\_H/TiO_2$ and $Ni_1(OH)_2/TiO_2$ can interconvert with each other easily and coexist. To ensure the stability of the $Ni_1(OH)_2/TiO_2$ catalyst in the hydrogenation reaction, the partial pressure of H_2O should be at least 10^{-3} atm.

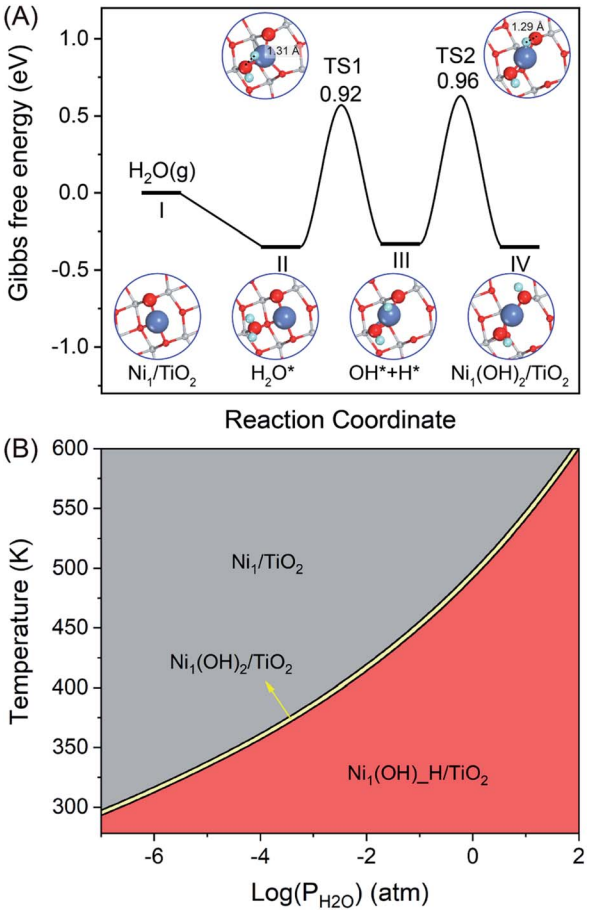

Fig. 1 (A) Gibbs free energy diagram and corresponding configurations for H_2O dissociation on Ni_1/TiO_2(101) in the formation of $Ni_1(OH)_2/TiO_2$(101) at T = 360 K and $P(H_2O)$ = 1 atm. Blue, grey, red and green balls are nickel, titanium, oxygen and hydrogen atoms, respectively. (B) Stability diagrams (difference in Gibbs free energy ΔG) of the Ni_1/TiO_2, $Ni_1(OH)\_H/TiO_2$ and $Ni_1(OH)_2/TiO_2$ catalysts as a function of temperature and partial pressure of H_2O.

Although the Ni adatom is bound to the TiO_2(101) surface strongly with the binding energy of −3.62 eV, it has high

mobility to aggregate into large nanoparticles on the $TiO_2(101)$ surface with a low diffusion barrier.[70] Furthermore, H_2 molecule heterolytically dissociates on Ni_1/TiO_2 is thermal neutral (-0.07 eV) that H_2 dissociative adsorption cannot compete with acetylene/ethylene adsorption, a fact that limits the overall reaction activity. However, the OH ligand bridges the Ni adatom and Ti on the oxide support with a higher atomic Ni diffusion barrier of 1.19 eV (Fig. S2†). The hydroxyl groups on the Ni_1/TiO_2 surface arises from the dissociation of steam, which stabilizes the single-atom Ni due to the strong interactions between Ni and OH. The two H in OH bridged Ni and Ti atoms are stable with the diffusion energies of 1.22 eV and 2.22 eV, respectively (Fig. S2†). Our calculation results are in line with many theoretical calculations and experimental studies which elucidate that transition metal atoms can be stabilized on the $TiO_2(101)$ surface *via* the interaction with excess O originating from the OH groups.[32,71,72] A large number of studies have shown that the presence of OH not only stabilizes single atom catalysts but also serves as an intermediate in the chemical reaction cycle.[45–47,73] The function of OH ligands, which can also serve as an intermediate in the chemical reaction cycle,[45–47,73] in the stable $Ni_1(OH)_2/TiO_2$ catalyst for catalyzing acetylene hydrogenation is extensively studied in the present work.

Adsorption of acetylene and ethylene

The adsorption strength and competitive adsorption of acetylene and ethylene determine the activity and selectivity of acetylene hydrogenation. Acetylene prefers to adsorb on the Ni (111) surface following the μ-bridge adsorption mode with the Gibbs free energy of -2.12 eV, whereas ethylene favors the perpendicular-bridge adsorption mode with the adsorption strength -0.57 eV weaker under reaction conditions (Fig. S3 and Table S1†). Ethylene adsorption is insensitive to the number of bound Ni atoms ranging from 1, 2 to 3. In contrast, the acetylene adsorption strength decreases with the decreasing number of bound Ni atoms ranging from 1 to 4. As a result, the adsorption difference between ethylene and acetylene at their most stable configurations is -1.55 eV, and becomes -0.08 eV in the π-bonded adsorption mode. The great change in competitive deficiency between acetylene and ethylene adsorption will have a tremendous impact on the selectivity of the acetylene hydrogenation reaction over Ni_1 catalysts, where acetylene and ethylene have the same π-bonded adsorption configuration.

Similar to the same π-bonded adsorption configuration on the Ni (111) surface, ethylene and acetylene have similar adsorption energies under reaction conditions ($G_{ads} = -0.68$ eV *vs.* -0.43 eV, Fig. 2 and Table S2†) on Ni_1/TiO_2. Therefore, Ni_1/TiO_2 will not be a good catalyst in acetylene hydrogenation because of the competitive hydrogenation of ethylene and acetylene resulting in poor selectivity of acetylene hydrogenation towards ethylene. Different from Ni_1/TiO_2, acetylene is adsorbed much more strongly than ethylene on the $Ni_1(OH)_2/TiO_2$ catalyst by 0.56 eV, conforming to the catalyst screening rule for acetylene semi-hydrogenation[14,74] which states that the large difference in acetylene and ethylene adsorption strength

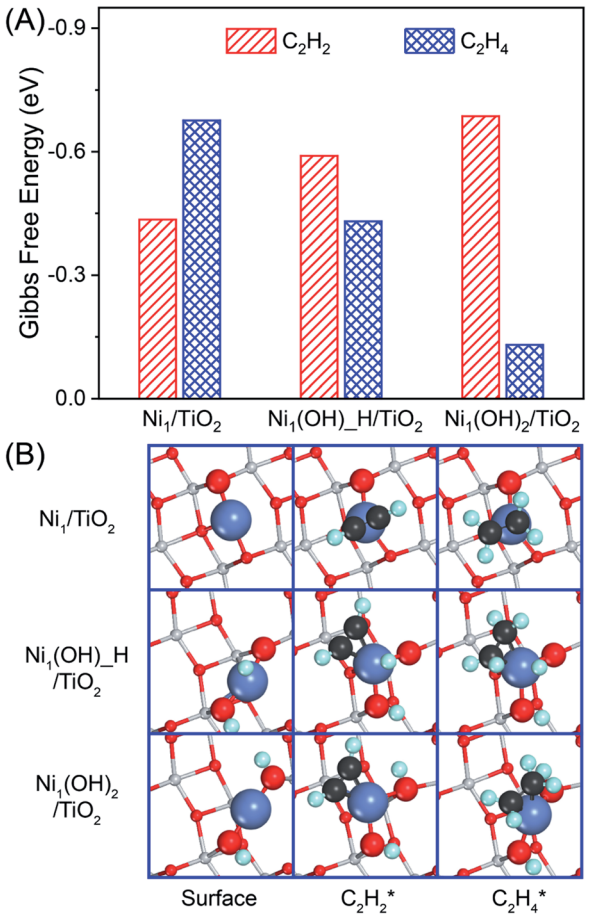

Fig. 2 Calculated adsorption energies with Gibbs free energy correction on reaction conditions (A) and the corresponding adsorption configurations (B) of C_2H_2 and C_2H_4 on Ni_1/TiO_2, $Ni_1(OH)\_H/TiO_2$ and $Ni_1(OH)_2/TiO_2$. Reaction conditions: $T = 360$ K, $P = 0.1$ MPa with 0.5% C_2H_2, 25% C_2H_4 and 5% H_2. Color code: Ni (blue), C (black), H (green), Ti (gray), O (red).

results in high selectivity in acetylene semi-hydrogenation towards ethylene. The presence of OH ligands modulates the electronic structure of the Ni atom in $Ni_1(OH)_2/TiO_2$, which has different catalytic behavior as compared with Ni_1/TiO_2, namely, acetylene adsorbs at the top of the Ni single atom in Ni_1/TiO_2 and at the side of the Ni single atom in $Ni_1(OH)_2/TiO_2$ (Fig. 2B and Table S2†).

To reveal the reason behind the adsorption energies of acetylene and ethylene having an opposite trend on Ni_1/TiO_2, and $Ni_1(OH)_2/TiO_2$, we resort to integrated COHP(ICOHP), a parameter that describes the bonding strength between reactants and the surface (Table S3†), and decompose the adsorption energy into the adsorption induced structure distortion cost E_{dis} and the chemical bonding energy gain E_b between the adsorbate and catalyst (Fig. S4†). For ethylene on Ni_1/TiO_2 and $Ni_1(OH)_2/TiO_2$, the corresponding – ICOHP is 1.59 eV and 1.65 eV. Comparable – ICOHP values indicate similar bonding strengths E_b between ethylene and the two catalysts (-2.00 eV, and -1.96 eV), in contrast to their large difference in E_{ads}, -0.79 eV for $Ni_1(OH)_2/TiO_2$ *vs.* -1.39 eV for Ni_1/TiO_2. The

less exothermic E_{ads} of ethylene on the former one is due to its larger distortion cost E_{dis}, 1.17 eV *vs.* 0.62 eV. For acetylene adsorption, though the distortion cost on $Ni_1(OH)_2/TiO_2$ (2.58 eV) remains larger than that on Ni_1/TiO_2 (0.76 eV), the corresponding – ICOHP is much larger, 2.25 eV *vs.* 1.69 eV. In fact, the calculated bonding energy E_b of acetylene on $Ni_1(OH)_2/TiO_2$ is −4.02 eV, significantly stronger than that on Ni_1/TiO_2 (−1.92 eV). This results in an overall more exothermic adsorption E_{ads}, −1.44 eV for $Ni_1(OH)_2/TiO_2$ *vs.* −1.16 eV for Ni_1/TiO_2, with an opposite trend to ethylene adsorption.

Hydrogenation of acetylene over the $Ni_1(OH)_2/TiO_2$ catalyst

We studied the mechanism of acetylene hydrogenation towards ethane over the $Ni_1(OH)_2/TiO_2$ catalyst. According to our DFT calculation results (Table S2†), the Ni single atom sites in the $Ni_1(OH)_2/TiO_2$ catalyst prefer to adsorb acetylene rather than H_2 and ethylene. The strongly competitive adsorption of acetylene compensates for the deficiency of the partial pressure of acetylene, improving the activity and selectivity of acetylene semi-hydrogenation thermodynamically. This is consistent with the rules for screening catalysts in previous literature.[14,74] For an acetylene presorbed $Ni_1(OH)_2/TiO_2$ catalyst, there are fewer active sites and less space for dissociation of physisorbed H_2 into atomic H species. Therefore, H atoms in OH ligands can serve as the hydrogen source in acetylene hydrogenation. Through systematic evaluation (Fig. 3, S5 and S6†), the optimal potential energy surface and the corresponding configurations involved in acetylene hydrogenation are shown in Fig. 3 and S5;† H in the bridged OH firstly diffuses to the acetylene adsorbed Ni single atom endothermically ($\Delta G = 0.12$ eV) with an activation barrier of 0.49 eV (I → II). After, the reaction of acetylene with the H at the Ni single atom site is highly exothermic ($\Delta G = -0.78$ eV) and much feasible with the activation barrier of 0.09 eV (II → III). Then, the formed $C_2H_3^*$ (* refers to the adsorption site) species can react with the physisorbed H_2 molecule generating $C_2H_4^*$ and leaving the second H atom still bound to the Ni single adatom (IV → V). This step is facile and highly exothermic, with an activation barrier of 0.33 eV and a reaction energy of −0.63 eV. Finally, the H atom bound to the Ni single atom site diffuses to the O atom forming OH (V → VI) endothermically by 0.28 eV with an activation energy barrier of 0.29 eV to recover the $Ni_1(OH)_2/TiO_2$ structure adsorbing ethylene. Although $C_2H_5^*$(VII) has a lower Gibbs free energy in the potential energy surface, it will not block the active site because the reverse reaction of $C_2H_5^*$ dehydrogenation to $C_2H_4^*$ has an activation barrier of 0.60 eV (Fig. S7†) which is still low to overcome at the typical temperature (360 K)

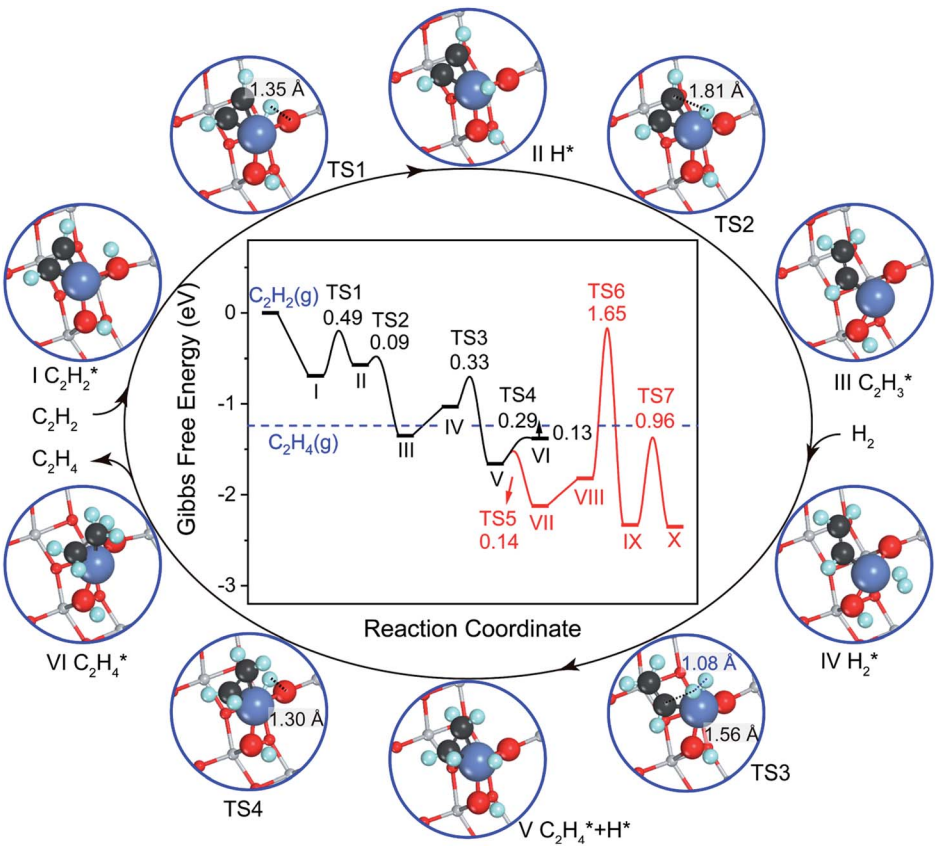

Fig. 3 Gibbs free energy diagram and corresponding configurations for acetylene hydrogenation towards ethane on the $Ni_1(OH)_2/TiO_2(101)$ catalyst. The Gibbs free energy was corrected at 360 K in a total pressure of 0.1 MPa, for 0.5% C_2H_2, 25% C_2H_4 and 5% H_2, respectively. The configurations involved in ethylene hydrogenation to ethane following the red curve in the potential energy diagram are given in Fig. S4.† All the energies are calculated with respect to acetylene and the hydrogen molecule in the gas phase. The blue dashed line represents the ethylene in the gas phase. The distances between C and H atoms in the transition states are indicated in Å.

for the acetylene hydrogenation reaction. The formed $C_2H_4^*$ prefers desorption rather than further hydrogenation towards ethane due to the higher activation barriers in the formation of $C_2H_6^*$ species than that of ethylene desorption by 0.13 eV. Therefore, the $Ni_1(OH)_2/TiO_2$ catalyst exhibits high selectivity in acetylene hydrogenation towards ethylene. The migration of H from the OH ligand to Ni, which has the highest activation for acetylene hydrogenation towards ethylene over the $Ni_1(OH)_2/TiO_2$ catalyst, could be the rate-determining step in acetylene hydrogenation.

The charge states of Ni, OH and TiO_2 surfaces during acetylene hydrogenation were analysed. Only 0.38*e* transfers from Ni to the support/OH ligand in the $Ni_1(OH)_2/TiO_2$ system (Table S4†), where some of the electron 0.25*e* localize at lattice oxygen in TiO_2 and 0.15*e* localizes on six-coordinated Ti underneath the Ni atom in the $Ni_1(OH)_2/TiO_2$ catalyst. The charge state of Ni, Ti underneath the Ni atom and O coordinated with Ni varies less than 0.20*e* during the acetylene hydrogenation cycle such that no polarons could migrate during the entire acetylene hydrogenation reaction. These results clearly show that the magnetic moments of Ti and O atoms have a slight change before and after loading the Ni single atom as well as during the hydrogenation cycle in $Ni_1(OH)_2/TiO_2$ catalytic systems. The surface coverage of H on metal oxides and the effect of hydrogenation of the metal oxide surface, which is likely to occur under the hydrogenation procedure, on the catalytic performance were also systemically evaluated. We found that the presence of surface H does not have a great influence on the activity and selectivity of acetylene hydrogenation (Fig. S8 and S9†).

The single atom catalyst $Ni_1(OH)_2/TiO_2$ has different activity and selectivity of acetylene hydrogenation towards ethylene as compared with a nanoparticle catalyst represented with a Ni (111) surface. The Gibbs free energy diagram and corresponding configurations for acetylene hydrogenation over the Ni (111) surface are shown in Fig. S10.† On the Ni (111) surface, the ethylene hydrogenation barrier is comparable to its desorption energy such that ethylene is not the dominant product in acetylene hydrogenation. Therefore, the Ni (111) surface has a lower selectivity in acetylene hydrogenation towards ethylene as compared with the $Ni_1(OH)_2/TiO_2$ structure. Among others, the effective hydrogenation barrier on Ni (111) is much higher than that on $Ni_1(OH)_2/TiO_2$ by 0.45 eV (Fig. 4), which could have originated from the stronger acetylene and ethylene adsorption strength on Ni (111) as compared with the $Ni_1(OH)_2/TiO_2$ catalyst. As a result, $Ni_1(OH)_2/TiO_2$ has superior performance to Ni nanoparticles not only in selectivity but also in reactivity.

As stated above, the hydrogenation of acetylene in the formation of $C_2H_3^*$ has an even lower activation barrier than $C_2H_5^*$ over the $Ni_1(OH)_2/TiO_2$ catalyst, because the Ni adatom and adsorbed $C_2H_3^*$ and $C_2H_5^*$ construct an interface that fulfills the formation of Frustrated Lewis Pairs (FLP)[75,76] and $C_2H_3^*/C_2H_5^*$ can serve as a basic ligand to accelerate the heterolytic dissociation of H_2. The hydrogenation of $C_2H_5^*$ has a higher activation barrier than that of $C_2H_3^*$ by 1.32 eV over the $Ni_1(OH)_2/TiO_2$ catalyst, which is mainly attributed to their different basicity values. The basicity of C in $C_2H_3^*$ is more than that in $C_2H_5^*$ reflected from the Bader charge analysis, +0.34*e* for C in $C_2H_3^*$ and +0.18*e* for the C in $C_2H_5^*$ (Fig. S11A and B†), which results in a much lower activation barrier for $C_2H_3^*$ hydrogenation due to the strong electrostatic interactions between H and Ni at the corresponding transition state. Homolytic H_2 activation on the Ni site in pristine $Ni_1(OH)_2/TiO_2$ is inhibited due to a strongly endothermic reaction energy of 2.09 eV (Fig. S11C†), and the heterolytic dissociation of H_2 is aided by ligand dominant acetylene hydrogenation activity.

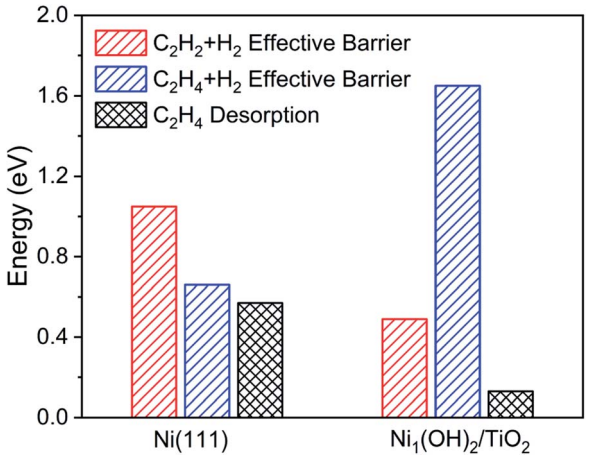

Fig. 4 The activity and selectivity comparisons between Ni (111) and $Ni_1(OH)_2/TiO_2$. The activity is represented by the effective hydrogenation barriers of acetylene. The selectivity for ethylene is estimated by comparing the difference between the desorption energies of ethylene and the effective hydrogenation barriers of ethylene. Reaction conditions: $T = 360$ K, $P = 0.1$ MPa with 0.5% C_2H_2, 25% C_2H_4 and 5% H_2.

The OH formed by H_2O dissociation anchors on the single Ni atom, inhibiting the migration and aggregation of the single Ni adatom. Modulating the electronic structure of Ni atoms by OH ligands enhances the adsorption strength of acetylene accompanied by weakening ethylene adsorption strength, which enlarges the adsorption energy difference between acetylene and ethylene, and improves the activity and selectivity of the catalyst thermodynamically. Hydrogen dissociative adsorption is often the rate-limiting step for single atom catalysts due to the limited space available for H_2 adsorption and activation. The formation of the $Ni - C_2H_3^*$ interface aided by adsorbed acetylene combined with H in the OH ligand led to the formation of effective Frustrated Lewis Pairs (FLP) and enabled more facile heterolytic dissociation of H_2, thus promoting the reactivity kinetically. Since stabilization of the $Ni_1(OH)_2$ complexes occurs on the whole TiO_2 surfaces, rather than on limited defect or step edge sites, a high loading of active $Ni_1(OH)_2/TiO_2$ can be achieved, one of the central challenges in single atom catalysts. All these together make $Ni_1(OH)_2/TiO_2$ a promising, stable, highly loaded, active and selective single atom catalyst for partial hydrogenation.

Comparison with other transition metals and more oxide supports

To reveal the uniqueness of $Ni_1(OH)_2/TiO_2$, we considered other transition metal catalysts including Co, Rh, Ir, Ni, Pd, Pt, Cu, Ag,

and Au, and more oxide surfaces including $Ni_1(OH)_2/MO_2$ (M = Zr, Ti, Nb and Ir). According to the optimal structure of the Ni single atom bound with two OH ligands in $Ni_1(OH)_2/TiO_2$, we further studied various $M_1(OH)_2/TiO_2$ catalysts (M = Co, Cu, Rh, Pd, Ag, Ir, Pt and Au) which have different electronic structures as compared with $Ni_1(OH)_2/TiO_2$. The stabilities of $M_1(OH)_2/TiO_2$ catalysts were first evaluated based on their formation energies which reflects the ability in the formation of the $M_1(OH)_2/TiO_2$ catalyst by steam treatment of the nanoparticles. The formation of $M_1(OH)_2/TiO_2$ can be calculated using:

$$E_f = E_{TM_1(OH)_2/TiO_2} - E_{NP} - E_{TiO_2} - E_{H_2O} \quad (5)$$

where E_{NP}, E_{TiO_2}, E_{H_2O} and $E_{TM_1(OH)_2/TiO_2}$ are the energies of metal nanoparticles (NP), the clean $TiO_2(101)$ surface, gaseous H_2O and the $TiO_2(101)$ supported TM_1 catalyst modulated by OH ligands, respectively. The total energy of a metal nanoparticle was corrected by eqn (6) as reported in previous literature:[77]

$$E_{NP} = E_{bulk\text{-}DFT} + \frac{3\Omega\gamma}{R} \quad (6)$$

where $E_{bulk\text{-}DFT}$ is the DFT calculated energy of the NP in the bulk phase, Ω is the molar volume of a metal atom, and γ is the overall surface energy of the metal particle. R is the radius of the nanoparticle. $R = 0.7$ nm was used in the present work.

Positive values of $M_1(OH)_2/TiO_2$ formation energies indicate that the formation of atomically dispersed catalysts is thermodynamically unfavorable, *vice versa*. Among all nine considered metals, $Cu_1(OH)_2/TiO_2$ is energetically most favorable, followed by $Ni_1(OH)_2/TiO_2$. However $Ir_1(OH)_2/TiO_2$ is least stable and highly endothermic. The stability of $M_1(OH)_2/TiO_2$ is determined by the interactions between the metal single atom and O (Table S5 and Fig. S12†). We note that although formation of $Cu_1(OH)_2/TiO_2$ is most favorable, the ethylene adsorption is stronger than that of acetylene, a fact that prevents effective acetylene hydrogenation (Table S6†).

The support effect on the stability of $Ni_1(OH)_2/MO_2$ (M = Zr, Ti, Nb and Ir) catalysts was further studied. Similar to $Ni_1(OH)_2/TiO_2$, the stability of $Ni_1(OH)_2/MO_2$ catalysts was defined as below:

$$E_f = E_{Ni_1(OH)_2/MO_2} - E_{NP} - E_{MO_2} - E_{H_2O} \quad (7)$$

where E_{NP}, E_{MO_2}, E_{H_2O} and $E_{Ni_1(OH)_2/MO_2}$ are the energies of the metal nanoparticle in the bulk phase, the clean metal oxide (101) surface, gaseous H_2O and the $Ni_1(OH)_2/MO_2$ catalyst, respectively.

It can be found that the $Ni_1(OH)_2/IrO_2$ catalyst has the highest stability, followed by $Ni_1(OH)_2/NbO_2$ and $Ni_1(OH)_2/TiO_2$ catalysts. However $Ni_1(OH)_2/ZrO_2$ is least stable among all four different metal oxide supported Ni single atom catalysts (Fig. 5B). The stability order of $Ni_1(OH)_2/MO_2$ catalysts is opposite to the order of the metal oxide formation energy (IrO_2 < NbO_2 < TiO_2 < ZrO_2). This could have originated from the fact that the stronger the interactions between metal and O in the host oxide surface, the less the energy gain to form a chemical bond toward Ni. For $Ni_1(OH)_2/IrO_2$, we found that acetylene and ethylene tend to adsorb at the exposed Ir atom, rather on the Ni_1 sites (Table S6†). A similar observation was made for $Ni_1(OH)_2/NbO_2$. The corresponding reactivity for acetylene hydrogenation is out of the scope of the present work.

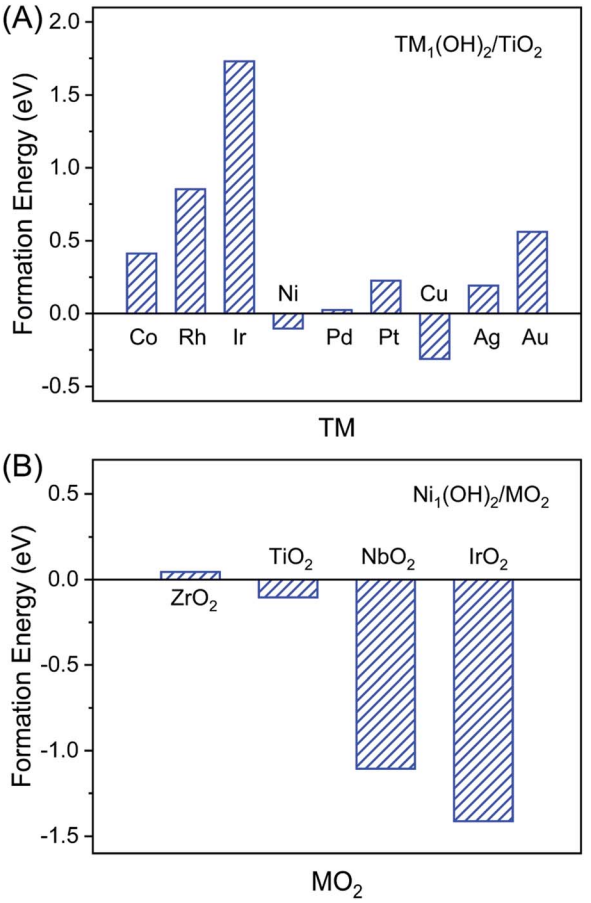

Fig. 5 The formation energies of $TM_1(OH)_2/TiO_2$ (TM = Co, Cu, Ni, Rh, Pd, Ag, Ir, Pt and Au) (A) and $Ni_1(OH)_2/MO_2$ (M = Zr, Ti, Nb and Ir) (B) by steam-treated corresponding metal nanoparticles.

Conclusions

DFT calculations reveal that hydroxyls present widely in catalytic systems can stabilize Ni single atoms on the anatase $TiO_2(110)$ surface efficiently. The resulting $Ni_1(OH)_2/TiO_2$ catalyst shows high activity for acetylene hydrogenation because its unique electronic and geometric structures form favourable bonds with acetylene and dissociates H_2 actively at the same time. Importantly, its weak bonding to ethylene facilitates the subsequent desorption achieving high selectivity toward ethylene. The uniqueness of $Ni_1(OH)_2/TiO_2$ is attributed to the synergy of stabilizing single transition metal atoms and modulating acetylene and ethylene adsorption. Our work demonstrates a promising strategy to utilize appropriate ligands forming new interfacial sites to mitigate competitive adsorption and molecular activation over atomically dispersed metal catalysts and revealed insights that could be used as guidelines for design of highly stable atomically dispersed

catalysts for acetylene hydrogenation on metal oxide materials without sacrificing activity.

Author contributions

Wei-Xue Li and Jin-Xun Liu led the conceptualization, design of DFT calculations, analysis and validation of the results. Minzhen Jian contributed to the DFT calculations and data analysis. All the authors participated in writing the manuscript.

Conflicts of interest

There are no conflicts to declare.

Acknowledgements

This work was supported by the Key Technologies R&D Program of China (2018YFA0208603), the National Natural Science Foundation of China (91945302), the Chinese Academy of Sciences Key Project (QYZDJ-SSW-SLH054), the start-up funds of University of Science and Technology of China (KY2060000171), USTC Research Funds of the Double First-Class Initiative (YD2060002012) and high-performance computational resources provided by the University of Science and Technology of China (http://scc.ustc.edu.cn).

Notes and references

1 A. Borodziński and G. C. Bond, *Catal. Rev.*, 2006, **48**, 91.
2 M. Takht Ravanchi, S. Sahebdelfar and S. Komeili, *Rev. Chem. Eng.*, 2018, **34**, 215.
3 F. Zaera, *ACS Catal.*, 2017, **7**, 4947.
4 A. Borodziński and G. C. Bond, *Catal. Rev.*, 2008, **50**, 379.
5 S. A. Nikolaev, L. N. Zanaveskin, V. V. Smirnov, V. A. Averyanov and K. L. Zanaveskin, *Russ. Chem. Rev.*, 2009, **78**, 231.
6 A. J. McCue and J. A. Anderson, *Front. Chem. Sci. Eng.*, 2015, **9**, 142.
7 A. Bos and K. Westerterp, *Chem. Eng. Process.*, 1993, **32**, 1.
8 B. Bridier, N. Lopez and J. Perez-Ramirez, *Dalton Trans.*, 2010, **39**, 8412.
9 D. L. Trimm, I. O. Y. Liu and N. W. Cant, *Appl. Catal., A*, 2010, **374**, 58.
10 R. T. Vang, K. Honkala, S. Dahl, E. K. Vestergaard, J. Schnadt, E. Laegsgaard, B. S. Clausen, J. K. Norskov and F. Besenbacher, *Nat. Mater.*, 2005, **4**, 160.
11 D. L. Trimm, I. O. Y. Liu and N. W. Cant, *J. Mol. Catal. A: Chem.*, 2008, **288**, 63.
12 D. L. Trimm, I. O. Y. Liu and N. W. Cant, *J. Mol. Catal. A: Chem.*, 2009, **307**, 13.
13 C. S. Spanjers, J. T. Held, M. J. Jones, D. D. Stanley, R. S. Sim, M. J. Janik and R. M. Rioux, *J. Catal.*, 2014, **316**, 164.
14 F. Studt, F. Abild-Pedersen, T. Bligaard, R. Z. Sørensen, C. H. Christensen and J. K. Nørskov, *Science*, 2008, **320**, 1320.
15 D. L. Trimm, N. W. Cant and I. O. Y. Liu, *Catal. Today*, 2011, **178**, 181.
16 C. S. Spanjers, R. S. Sim, N. P. Sturgis, B. Kabius and R. M. Rioux, *ACS Catal.*, 2015, **5**, 3304.
17 Y. Niu, X. Huang, Y. Wang, M. Xu, J. Chen, S. Xu, M. G. Willinger, W. Zhang, M. Wei and B. Zhang, *Nat. Commun.*, 2020, **11**, 3324.
18 S. Zhou, L. Kang, X. Zhou, Z. Xu and M. Zhu, *Nanomaterials*, 2020, **10**, 509.
19 Y. Liu, J. Zhao, J. Feng, Y. He, Y. Du and D. Li, *J. Catal.*, 2018, **359**, 251.
20 H. Liu, M. Chai, G. Pei, X. Liu, L. Li, L. Kang, A. Wang and T. Zhang, *Chin. J. Catal.*, 2020, **41**, 1099.
21 M. Chai, X. Liu, L. Li, G. Pei, Y. Ren, Y. Su, H. Cheng, A. Wang and T. Zhang, *Chin. J. Catal.*, 2017, **38**, 1338.
22 S. A. Nikolaev and V. V. Smirnov, *Catal. Today*, 2009, **147**, S336.
23 S. A. Nikolaev, V. V. Smirnov, A. Y. Vasil'kov and V. L. Podshibikhin, *Kinet. Catal.*, 2010, **51**, 375.
24 Y. Cao, H. Zhang, S. Ji, Z. Sui, Z. Jiang, D. Wang, F. Zaera, X. Zhou, X. Duan and Y. Li, *Angew. Chem., Int. Ed. Engl.*, 2020, **59**, 11647.
25 D. M. Rao, S. T. Zhang, C. M. Li, Y. D. Chen, M. Pu, H. Yan and M. Wei, *Dalton Trans.*, 2018, **47**, 4198.
26 Q. Li, Y. Wang, G. Skoptsov and J. Hu, *Ind. Eng. Chem. Res.*, 2019, **58**, 20620.
27 A. Onda, T. Komatsu and T. Yashima, *Phys. Chem. Chem. Phys.*, 2000, **2**, 2999.
28 Y. Liu, X. Liu, Q. Feng, D. He, L. Zhang, C. Lian, R. Shen, G. Zhao, Y. Ji, D. Wang, G. Zhou and Y. Li, *Adv. Mater.*, 2016, **28**, 4747.
29 D. Teschner, J. Borsodi, A. Wootsch, Z. Révay, M. Hävecker, A. Knop-Gericke, S. D. Jackson and R. Schlögl, *Science*, 2008, **320**, 86.
30 M. Akri, S. Zhao, X. Li, K. Zang, A. F. Lee, M. A. Isaacs, W. Xi, Y. Gangarajula, J. Luo, Y. Ren, Y. T. Cui, L. Li, Y. Su, X. Pan, W. Wen, Y. Pan, K. Wilson, L. Li, B. Qiao, H. Ishii, Y. F. Liao, A. Wang, X. Wang and T. Zhang, *Nat. Commun.*, 2019, **10**, 5181.
31 F. Huang, Y. Deng, Y. Chen, X. Cai, M. Peng, Z. Jia, P. Ren, D. Xiao, X. Wen, N. Wang, H. Liu and D. Ma, *J. Am. Chem. Soc.*, 2018, **140**, 13142.
32 L. DeRita, J. Resasco, S. Dai, A. Boubnov, H. V. Thang, A. S. Hoffman, I. Ro, G. W. Graham, S. R. Bare and G. Pacchioni, *Nat. Mater.*, 2019, **18**, 746.
33 Y. Pan, Y. Chen, K. Wu, Z. Chen, S. Liu, X. Cao, W.-C. Cheong, T. Meng, J. Luo, L. Zheng, C. Liu, D. Wang, Q. Peng, J. Li and C. Chen, *Nat. Commun.*, 2019, **10**, 1.
34 W. Liu, L. Zhang, X. Liu, X. Liu, X. Yang, S. Miao, W. Wang, A. Wang and T. Zhang, *J. Am. Chem. Soc.*, 2017, **139**, 10790.
35 C. Martinez-Macias, P. Serna and B. C. Gates, *ACS Catal.*, 2015, **5**, 5647.
36 H. Yan, X. Zhao, N. Guo, Z. Lyu, Y. Du, S. Xi, R. Guo, C. Chen, Z. Chen, W. Liu, C. Yao, J. Li, S. J. Pennycook, W. Chen, C. Su, C. Zhang and J. Lu, *Nat. Commun.*, 2018, **9**, 3197.
37 P. Liu and N. Zheng, *Natl. Sci. Rev.*, 2018, **5**, 636.
38 X. Dai, Z. Chen, T. Yao, L. Zheng, Y. Lin, W. Liu, H. Ju, J. Zhu, X. Hong and S. Wei, *Chem. Commun.*, 2017, **53**, 11568.

39 Y. Chai, G. Wu, X. Liu, Y. Ren, W. Dai, C. Wang, Z. Xie, N. Guan and L. Li, *J. Am. Chem. Soc.*, 2019, **141**, 9920.
40 L. Liu and A. Corma, *Chem. Rev.*, 2018, **118**, 4981.
41 L. Zhang, M. Zhou, A. Wang and T. Zhang, *Chem. Rev.*, 2019, **120**, 683.
42 G. Kyriakou, M. B. Boucher, A. D. Jewell, E. A. Lewis, T. J. Lawton, A. E. Baber, H. L. Tierney, M. Flytzani-Stephanopoulos and E. C. H. Sykes, *Science*, 2012, **335**, 1209.
43 P. Liu, Y. Zhao, R. Qin, S. Mo, G. Chen, L. Gu, D. M. Chevrier, P. Zhang, Q. Guo, D. Zang, B. Wu, G. Fu and N. Zheng, *Science*, 2016, **352**, 797.
44 Y. Lu, J. Wang, L. Yu, L. Kovarik, X. Zhang, A. S. Hoffman, A. Gallo, S. R. Bare, D. Sokaras, T. Kroll, V. Dagle, H. Xin and A. M. Karim, *Nat. Catal.*, 2018, **2**, 149.
45 L. Cao, W. Liu, Q. Luo, R. Yin, B. Wang, J. Weissenrieder, M. Soldemo, H. Yan, Y. Lin, Z. Sun, C. Ma, W. Zhang, S. Chen, H. Wang, Q. Guan, T. Yao, S. Wei, J. Yang and J. Lu, *Nature*, 2019, **565**, 631.
46 M. Jian, C. Zhao and W. X. Li, *ChemPhysChem*, 2020, **21**, 2417.
47 H. Jeong, G. Lee, B. S. Kim, J. Bae, J. W. Han and H. Lee, *J. Am. Chem. Soc.*, 2018, **140**, 9558.
48 R. Addou, T. P. Senftle, N. O'Connor, M. J. Janik, A. C. T. van Duin and M. Batzill, *ACS Nano*, 2014, **8**, 6321.
49 G. S. Parkinson, Z. Novotny, G. Argentero, M. Schmid, J. Pavelec, R. Kosak, P. Blaha and U. Diebold, *Nat. Mater.*, 2013, **12**, 724.
50 S. Tosoni and G. Pacchioni, *Surf. Sci.*, 2017, **664**, 87.
51 S. Riyapan, Y. Boonyongmaneerat, O. Mekasuwandumrong, H. Yoshida, S.-I. Fujita, M. Arai and J. Panpranot, *J. Mol. Catal. A: Chem.*, 2014, **383**, 182.
52 S. Riyapan, Y. Boonyongmaneerat, O. Mekasuwandumrong, P. Praserthdam and J. Panpranot, *Catal. Today*, 2015, **245**, 134.
53 M. Lazzeri, A. Vittadini and A. Selloni, *Phys. Rev. B: Condens. Matter Mater. Phys.*, 2001, **63**, 155409.
54 C. Arrouvel, M. Digne, M. Breysse, H. Toulhoat and P. Raybaud, *J. Catal.*, 2004, **222**, 152.
55 A. S. Barnard, P. Zapol and L. A. Curtiss, *Surf. Sci.*, 2005, **582**, 173.
56 A. S. Barnard and P. Zapol, *Phys. Rev. B: Condens. Matter Mater. Phys.*, 2004, **70**, 235403.
57 G. Kresse and J. Furthmüller, *Comput. Mater. Sci.*, 1996, **54**, 11169.
58 G. Kresse and J. Furthmüller, *Comput. Mater. Sci.*, 1996, **6**, 15.
59 J. Klimeš, D. R. Bowler and A. Michaelides, *Phys. Rev. B: Condens. Matter Mater. Phys.*, 2011, 83.
60 A. O'Hara, T. N. Nunley, A. B. Posadas, S. Zollner and A. A. Demkov, *J. Appl. Phys.*, 2014, 116.
61 F. G. Sen, A. Kinaci, B. Narayanan, S. K. Gray, M. J. Davis, S. K. R. S. Sankaranarayanan and M. K. Y. Chan, *J. Mater. Chem. A*, 2015, **3**, 18970.
62 H.-Y. T. Chen, S. Tosoni and G. Pacchioni, *Surf. Sci.*, 2016, **652**, 163.
63 G. Kresse and D. Joubert, *Phys. Rev. B: Condens. Matter Mater. Phys.*, 1999, **59**, 1758.
64 G. Henkelman and H. Jónsson, *J. Chem. Phys.*, 2000, **113**, 9978.
65 G. Henkelman, B. P. Uberuaga and H. Jónsson, *J. Chem. Phys.*, 2000, **113**, 9901.
66 J. Kastner and P. Sherwood, *J. Chem. Phys.*, 2008, **128**, 014106.
67 Y. Wang, Y. Su, M. Zhu and L. Kang, *RSC Adv.*, 2015, **5**, 16582.
68 Y. Han, C.-j. Liu and Q. Ge, *J. Phys. Chem. B*, 2006, **110**, 7463.
69 J. Zhang, M. Zhang, Y. Han, W. Li, X. Meng and B. Zong, *J. Phys. Chem. C*, 2008, **112**, 19506.
70 A. Alghannam, C. L. Muhich and C. B. Musgrave, *Phys. Chem. Chem. Phys.*, 2017, **19**, 4541.
71 H. V. Thang and G. Pacchioni, *J. Phys. Chem. C*, 2019, **123**, 7271.
72 H. V. Thang, G. Pacchioni, L. DeRita and P. Christopher, *J. Catal.*, 2018, **367**, 104.
73 L. Nie, D. Mei, H. Xiong, B. Peng, Z. Ren, X. I. P. Hernandez, A. DeLaRiva, M. Wang, M. H. Engelhard, L. Kovarik, A. K. Datye and Y. Wang, *Science*, 2017, **358**, 1419.
74 F. Studt, F. Abild-Pedersen, T. Bligaard, R. Z. Sørensen, C. H. Christensen and J. K. Nørskov, *Angew. Chem.*, 2008, **120**, 9439.
75 G. Lu, P. Zhang, D. Sun, L. Wang, K. Zhou, Z.-X. Wang and G.-C. Guo, *Chem. Sci.*, 2014, **5**, 1082.
76 J. L. Fiorio, N. López and L. M. Rossi, *ACS Catal.*, 2017, **7**, 2973.
77 R. Ouyang, J. X. Liu and W. X. Li, *J. Am. Chem. Soc.*, 2013, **135**, 1760.